

¹ Multiple Site Age-Depth Distribution Estimation using
² Paleoperspectives from Barley Lake, CA

³ Kevin Nichols¹, Reza Ramezan ², Seth Arreola ¹, Matthew Kirby ³, Glen
⁴ MacDonald⁴, Joe Carlin³, Jennifer Leidelmeijer - still at CSUF but
⁵ graduated ³, Judith Agila now at University of Minnesota - see Leidelmeijer
⁶ paper³, Jiwoo Han³, Benjamin Nauman³, Sean Loyd³

⁷ *1: Corresponding Author*
⁸ *CSUF Department of Mathematics*
⁹ *800 North State College Blvd*
¹⁰ *Fullerton, CA 92831*

¹¹ *2: University of Waterloo Department of Mathematics*

¹² *3: CSUF Department of Geological Sciences*

¹³ *4: UCLA Department of Geology - see Leidelmeijer et al. 2021 for correct UCLA contact*
¹⁴ *information*

¹⁵ **Abstract**

¹⁶ Of key importance when it comes to re-constructing past climate is the
¹⁷ ability to collect data, harvest that data into information, and finally to
¹⁸ compile that information into a coherent narrative. Key to developing this
¹⁹ narrative is the quantity and quality of age control data. Lake sediment
²⁰ paleoclimatic narratives use age models to infer an age-depth relationship.
²¹ Often, these lacustrine sediment age models rely on radiocarbon dates used
²² to generate a probabilistic representation of age versus depth (age depth
²³ model references). Often the dates of important paleoclimatic events such as
²⁴ droughts, floods, fires, and pluvials are represented as a probability density
²⁵ function via age depth modeling. However, most lacustrine sediment-based
²⁶ age depth models rely on radiocarbon dating, and there are potentials age
²⁷ modelling errors associated with stratigraphic inversions, hiatuses, too few
²⁸ age data, and carbon contamination (carbon contamination references). In
²⁹ fact, cores from neighboring lakes or even separate cores within the same lake
³⁰ can result in contradictory narratives with regards to the dates of important
³¹ paleoclimatic events. It becomes imperative for the science to be able to effi-

ciently combine probability density functions resulting from several different sediment cores to produce a single narrative on the distribution of these important events; preferably, a narrative that minimizes the representation of biased samples and accentuates the representation of unbiased ones. This paper develops a method for estimating the probability density function for the duration of a purported sediment hiatus (i.e., severe drought) during the late Holocene in central California. New statistical methodology for combining probability functions into a single probabilistic representation is introduced. The new methodology is vetted with synthetic data in which various levels of bias are introduced. Finally, the utility of the new methodology is displayed via four lacustrine sediment cores from Barley lake, CA. Preliminary results indicate with a large number of dated sediment cores from the same site, biased samples play a minimal role in a collective narrative. However, with a smaller number of samples, one or two moderately biased samples can significantly impact the joint narrative.

Keywords: Keyword1, Keyword2, Keyword3

1. Introduction

Paleo-perspectives on climate and perhaps more importantly climate change are critical in contextualizing modern impacts on climate in that historical perspectives provide relevant baselines for comparison. Key to these paleo-perspectives is high-resolution and high quality age control. For many late Quaternary studies, this age control is based on radiocarbon dating of discrete organic materials preserved in various geological archives, such as lake sediments. Age-depth models like BACON (REFERENCE FOR BACON), are critical in forming these paleo-perspectives as they translate radiocarbon ages determined from a lacustrine sediment core into a probabilistic representation of age. It is evident that some of these probability distributions are impacted by biases when it comes to representing the age probability distribution of notable events. For example, a long period of drought, as separated local samples often have non-overlapping probability distributions.

This research focuses on adapting the output of age-depth models such as that generated using BACON to cohesively develop a joint paleo-perspective based on multiple, radiocarbon dated sediment cores collected from the same lake study site (i.e., Barley Lake, CA). This research introduces a methodology for adapting BACON to determine a probability distribution for the

length of a hiatus, perhaps associated with extreme drought and low lake levels. Next, a second novel statistical methodology for harmonizing probability distributions, some of which may reflect biases of varying magnitude, into a single probability perspective is discussed. The latter methodology is vetted using a robust sets of simulated data. Finally the methodologies are applied to four radiocarbon dated, lacustrine cores from Barley Lake, CA.

2. Data

This paper highlights two separate sources of data. The first is synthetic data which is simulated to realistically mirror the complexity produced by event age estimation from Bacon (an age-depth model). The advantage of synthetic data is that the true probability distribution for the age of the event (f) is known and separate from estimation of that true distribution (\hat{f}) can be quantified using some objective measure of fit. In this case, the objective measure of fit is mean integrated squared error $\int_{-\infty}^{\infty} (f(x) - \hat{f}(x))^2 dx$

The second data source is four radiocarbon dated, sediment cores from Barley Lake, CA. The methodology is applied to this data to illustrate how competing narratives from as little as four samples can be reconciled by the methodology introduced in this paper so long as the data is rich.

2.1. Synthetic Data

The central focus of this research is to develop a method for synchronizing multiple data sources, emphasizing the roles of unbiased data, and marginalizing the roles of biased data. Towards this end, synthetic data is a useful tool for assessing method success in a variety of situations. Three distinct factors have the potential to impact method efficiency, as is measured by mean integrated squared error between the estimated density produced by the methodology and the true density from which the data was sampled. The three distinct factors are the number of data sources being synthesized (n), the number of biased data sources being synthesized (m), and the degree of bias in those data sources. The population density from which data sources are sampled is a normal distribution. Three different degrees of bias are potentially implemented. An unbiased sample is sampled directly from the population which is $N(\mu, \sigma)$. A small bias sample is sampled from a $N(\mu + u, \sigma)$ where u is a uniformly distributed random variable over $[-\frac{2}{3}\sigma, \frac{2}{3}\sigma]$. A large bias sample is sampled from a $N(\mu + v, \sigma)$ where v is

101 a uniformly distributed random variable over $[-3\sigma, 3\sigma]$. Preliminary simulations
102 focus on mirroring localized data sources (n is small) vs regional data
103 sources (n is large) under varying counts and degrees of bias. Specifically the
104 seven scenarios considered are:

- 105 • Scenario (1): Four samples, no bias (Base Case, small n)
- 106 • Scenario (2): Four samples, one large bias (small n , small m)
- 107 • Scenario (3): Four samples, one small bias (small n , small m)
- 108 • Scenario (4): Four samples, two large biases (small n , large m)
- 109 • Scenario (5): Twenty samples, no bias (Base Case, large n)
- 110 • Scenario (6): Twenty samples, four large biases (large n , small m)
- 111 • Scenario (7): Twenty samples, ten large biases (large n , large m)

112 Under each scenario, data sources are sampled 1,000 times and the aver-
113 age mean integrated squared error is approximated via a Riemann integral
114 approximation.

115 *2.2. Barley Lake*

116 Four sediment cores were extracted from Barley Lake in 2017, a small
117 landslide formed basin ($N39^{\circ}35'30''$, $W122^{\circ}58'40''$), located in the Northern
118 California Coastal Range (1,658 masl) (Figure 1). Cores BLRC17-1 and
119 -2 were extracted from the center of the modern lake, while core BLRC17-
120 3 and -4 were extracted from near the modern edge of the lake. When
121 sampled in August 2017, Barley Lake was approximately 0.13km in length
122 and approximately 0.08km in width with a drainage basin of approximately
123 0.13km² and a maximum depth of approximately 0.5m. Presently, the lake
124 is shallow and highly productive. However, Leidelmeijer et al. (2021) found
125 evidence for a deeper, lower productivity lake during the late last Glacial
126 (i.e., the Younger Dryas [12.9-11.7 ka]). At the end of the Younger Dryas
127 (YD), the lake abruptly shifted to its present shallow, highly productive
128 state. This finding demonstrates the hydroclimatic sensitivity of northern
129 CA climate, as continued through present day. s((Adam and West, 1983;
130 Rypins et al., 1989; West, 1993; Heusser, 1998; Mohr et al., 2000; Barron et
131 al., 2003; Daniels et al., 2005; Vacco et al., 2005; Briles et al., 2008; Ersek et

al., 2012; Anderson et al., 2020). Yet unpublished sediment data from the same Barley Lake core shows evidence for hydroclimatic variability within the "stable" Holocene, indicating that abrupt hydrologic changes are not unique to the YD-Holocene transition. For example, as shown in this paper, rapid changes in age-depth relationships in the late Holocene suggest a sustained period of aridity during which Barley Lake either desiccated (i.e., hiatus forming event) or remained very shallow. One of this paper's objectives is to interrogate this age-depth data using multiple, dated cores from Barley Lake and to assess the likelihood and timing of this purported late Holocene dry period.

For each of the four sediment cores, discrete organic materials \lesssim 125 microns were removed and dated using the AMS (accelerator mass spectrometry) radiocarbon method at the University of California, Irvine Keck-Carbon Cycle AMS facility (TABLE with ALL ages). For comparison, percent total organic matter for each core is plotted with their respective radiocarbon ages by depth (Figure 2). Relevant probability distributions for each radiocarbon date per depth were run through BACON to generate age-depth models (Blaauw and Christen, 2011). Figure 3 provides the average estimated age for radiocarbon dated materials in each of the four sampled cores; while, Figure 4 provides the estimated probability distributions of Bacon age-depth modeling on radiocarbon dated materials.

3. Statistical methodologies

Novel statistical approaches were developed to estimate the probability density of the duration of a drought or hiatus and to combine several probability densities for the same event into a single converged density.

3.1. Estimating late Holocene hiatus duration

Age depth models are constructed by interpolating a probability distribution for age $g(d^*)$ at a given depth d^* based on analyzed observed depths d_1, \dots, d_m where carbon samples have been analyzed via radio carbon dating processes (reference needed). Estimating the start point, end point or duration of a hiatus is computationally challenging as field specialists have a collection of points d_1, \dots, d_i prior to the start of the hiatus and points d_{i+1}, \dots, d_m following the hiatus. There are however no assurances that d_i nor d_{i+1} are the depths that mark the beginning and end of the hiatus respectively.

167 In order to estimate the distribution of the length of the hiatus $f()$ separate age depth models $g_1(d^*)$ and $g_2(d^*)$ are created for each core sample
 168 based on points prior to the hiatus d_1, \dots, d_i and points post-hiatus d_{i+1}, \dots, d_m .
 169 d^* is selected from the depth domain $[d_i, d_{i+1}]$, (for this research, d^* was simply set to d_i). 6,000 samples were drawn from both $g_1(d^*)$ and $g_2(d^*)$ with
 170 resulting differences computed. The end product is 6,000 bootstrapped samples of the difference in age at a depth close to beginning of the hiatus between
 171 an age depth model in which there is no hiatus and an age depth model in
 172 which there was a hiatus. This corresponds to 6,000 random samples from
 173 the joint probability distribution of the age $g(d^*)$ with or without the hiatus.
 174 Sampling from the joint distribution and then taking the difference in ages
 175 provides an empirical estimation of the distribution of the duration of the
 176 hiatus $f()$. Figure 5 provides an illustration of how the joint distribution of
 177 $g_1(d^*), g_2(d^*)$ can be empirical sampled from Bacon output.

181 3.2. Density congruence methodology

182 Once again, the primary purpose of this study it to produce a single narrative from multiple sources of data, which marginalizes biased sources. To
 183 produce such a narrative, a single probability density for the date or duration
 184 of a climate event is assumed (f). Using the aforementioned methodology
 185 for duration estimation, each sample results in a single density estimation
 186 or event narrative (\hat{f}_j). Our convergence algorithm combines the isolated
 187 narratives into one joint narrative (\hat{f}). \hat{f}_j is estimated via kernel density
 188 estimation (See Bowman et al. 1998, Zhang et al. 2004 for examples) where
 189 kernel bandwidth was selected via a 10-fold cross validation using MISE.
 190 The convergence algorithm begins by assuming equal weights on our k den-
 191 sity estimates $\hat{f}_1, \dots, \hat{f}_k$. $\hat{f}(x) = \sum_{j=1}^k W_j * \hat{f}_j(x)$ where W_j is the weight of
 192 \hat{f}_j in the estimation of \hat{f} . Mean integrated squared error ($I(j, i)$) for the
 193 i^{th} iteration of the algorithm is calculated for the j^{th} sample distribution
 194 $\hat{f}_j(x)$ with respect to our single estimated density $\hat{f}(x)$ and weights are up-
 195 dated as follows: $W_{j,i} = \alpha * (\frac{R_{j,i}}{\sum_{j=1}^n R_{j,i}}) + (1 - \alpha) * W_{j,i-i}$ where $W_{j,i}$ is the
 196 weight for the j^{th} sample distribution $\hat{f}_j(x)$ on the i^{th} iteration of this pro-
 197 cess. $R_{j,i} = \alpha * I(j, i) + (1 - \alpha) * R_{j,i-i}$ where α is a shrinkage parameter.
 198 Estimation of \hat{f} and each of the $W_{j,i}$'s is repeated until convergence.

200 **4. Results and Discussion**

201 *4.1. Synthetic Data*

202 Having discussed the methods of simulation previously, we can now ana-
203 lyze the performance of the method on synthetic data. Specifically we discuss
204 how this method fairs in respect to the three key factors mentioned, the num-
205 ber of data sources, the number of biased data sources, and the degree of bias
206 within each source. Note, results found here can also be viewed in Table 1,
207 which lists each scenario discussed under the methodology section and their
208 respected average mean integrated squared error per 1,000 simulations.

209 Scenarios (1-4) consider simulations which mirrored localized data sources
210 where the number of data sources being synthesized are small ($k=4$) while
211 scenarios (5-7) represent simulations in which data sources are more abun-
212 dant ($k=20$). Of these scenarios, scenario (1) and scenario (5) represent cases
213 with no sources of bias and thus provide relative baselines for performance.
214 Table 1 provides the relative MISE for all scenarios. From these simulated
215 results it's apparent when k is small a single biased source, irregardless of
216 the magnitude of bias has relatively no impact on overall estimation efficacy
217 as was simulated in scenarios 2 and 3 (see Figures 6 and 7). However, once
218 there are two sources of bias of reasonably large magnitude overall estimation
219 success is substantially impacted as was simulated in scenario 4 (see Figure
220 8). When k is large, the algorithm is robust if there are relatively few biased
221 sources as was simulated in scenario 6 (see Figure 9) and performs reasonably
222 well even with a high number of contaminated sources as was simulated in
223 scenario 7 (see Figure 10).

224 Overall, there is strong evidence that the correct probability distribution
225 of notable climate events will not be impeded by a few contaminated data
226 sources provided a large collective of data sources. However, with fewer data
227 sources, like we see in Barley Lake, even a few biased data sources can't be
228 mitigated when it comes to estimating the probability distribution of notable
229 events.

230 *4.2. Barley Lake*

231 Implementation of methodology for estimating the length of the late
232 Holocene hiatus yielded empirical distributions of $g_1(d^*)$ and $g_2(d^*)$ where
233 d^* was always selected as the endpoint preceding the late Holocene hiatus.
234 The bivariate distribution of g_1, g_2 is provided for each core in Figure 11,
235 while an empirical distribution for the estimated length of the hiatus based

236 on each core is provided in Figure 12. Estimation of the collaborative proba-
237 bility density function of the length of the late Holocene hiatus is illustrated
238 in Figure 13 along each cores probabilistic perspective on the hiatus length.
239 Note that the narrative provided by sample 3 is noticeably rejected by the
240 other three samples. Of the four sediment cores, sample 3 (core BLRC17-
241 3) was taken closest to shore. As a result, over the period of study (late
242 Holocene), this core may have been subject to more vigorous near shore en-
243 ergy dynamics such as wave action, resuspension, and reworking than the
244 other 3 cores. Together these latter processes often obfuscate the sediment
245 stratigraphy resulting in age reversals and/or reworked organic materials.
246 Consequently, it is not surprising that sample 3 is the most dissimilar of the
247 four core age distributions. Samples 2 and 4 show the most similar probabili-
248 ty distributions with sample 1 slightly less conformable.

249 It should be noted that in the context of our simulated efforts, there is
250 not much certainty that the narrative primarily supported by samples 2 and
251 4 is necessarily reflective of the true probability distribution for the duration
252 of the hiatus. With only four cores it is obvious that at least some of our
253 samples are reflecting bias but there is no evidence that any of our samples
254 are unbiased. By tying the data collected from Barley lake with other dated
255 sediment archives from Northern California the confidence in a joint narrative
256 on the duration of the hiatus can only grow. Such is the focus of critical next
257 steps in this research exploration.

258 References

- 259 [1] Botev, Z., J. Grotowski, D. Kroese, (2010). Kernel Density Estimation
260 Via Diffusion, *Annals of Statistics*, 38(5): 2916-2957. DOI: 10.1214/10-
261 AOS799

262 List of Figures and their Captions:

263 Table 1: Average Mean Integrated Squared Error per 1,000 Simulations
264 for each of the seven simulated data indices.

265 Figure 1: Map of Barley Lake with marked coring locations, BLRC17-
266 1,BLRC17-2,BLRC17-3,BLRC17-4.

267 Figure 2: Total Organic Matter % analyzed for each of the four Barley
268 Lake Lacustrine Cores.

269 Figure 3: Average Mean Age vs. Depth for carbon-dated organic mate-
270 rials across the four Barley Lake samples.

271 Figure 4: Bacon ghost plots empirically representing age-depth probabil-
272 ity densities for each of the four Barley Lake samples. Empirical distributions
273 represented by 6000 posterior samples from the MCMC algorithm.

274 Figure 5: Illustration of process for determining the Bivariate distribution
275 of $g_1(d^*), g_2(d^*)$ using BLRC17-1 and $d^* = 64.5$ cm.

276 Figure 6: Example result of density congruence methodology for scenario
277 (2).

278 Figure 7: Example result of density congruence methodology for scenario
279 (3).

280 Figure 8: Example result of density congruence methodology for scenario
281 (4).

282 Figure 9: Example result of density congruence methodology for scenario
283 (6).

284 Figure 10: Example result of density congruence methodology for scenario
285 (7).

286 Figure 11: Empirical Bivariate distribution of $g_1(d^*), g_2(d^*)$ for BLRC17-
287 1,BLRC17-2,BLRC17-3,BLRC17-4.

288 Figure 12: Estimated Probability Density functions for late Holocene
289 hiatus for BLRC17-1,BLRC17-2,BLRC17-3,BLRC17-4.

290 Figure 13: Estimated congruence distribution of the late Holocene hiatus
291 based on BLRC17-1,BLRC17-2,BLRC17-3,BLRC17-4.

Simulation	MISE
Simulation 1: Baseline (n=4, m=0)	7.848e-05
Simulation 2: (n=4, m=1)	9.180e-05
Simulation 3: (n=4, m=1)	8.995e-05
Simulation 4: (n=4, m=2)	5.711e-03
Simulation 5: Baseline (n=20, m=0)	4.073e-05
Simulation 6: (n=20, m=4)	2.695e-04
Simulation 7: (n=20, m=10)	2.415e-03

Table 1: Average Mean Integrated Squared Error per 1,000 Simulations for each of the seven simulated data indices.

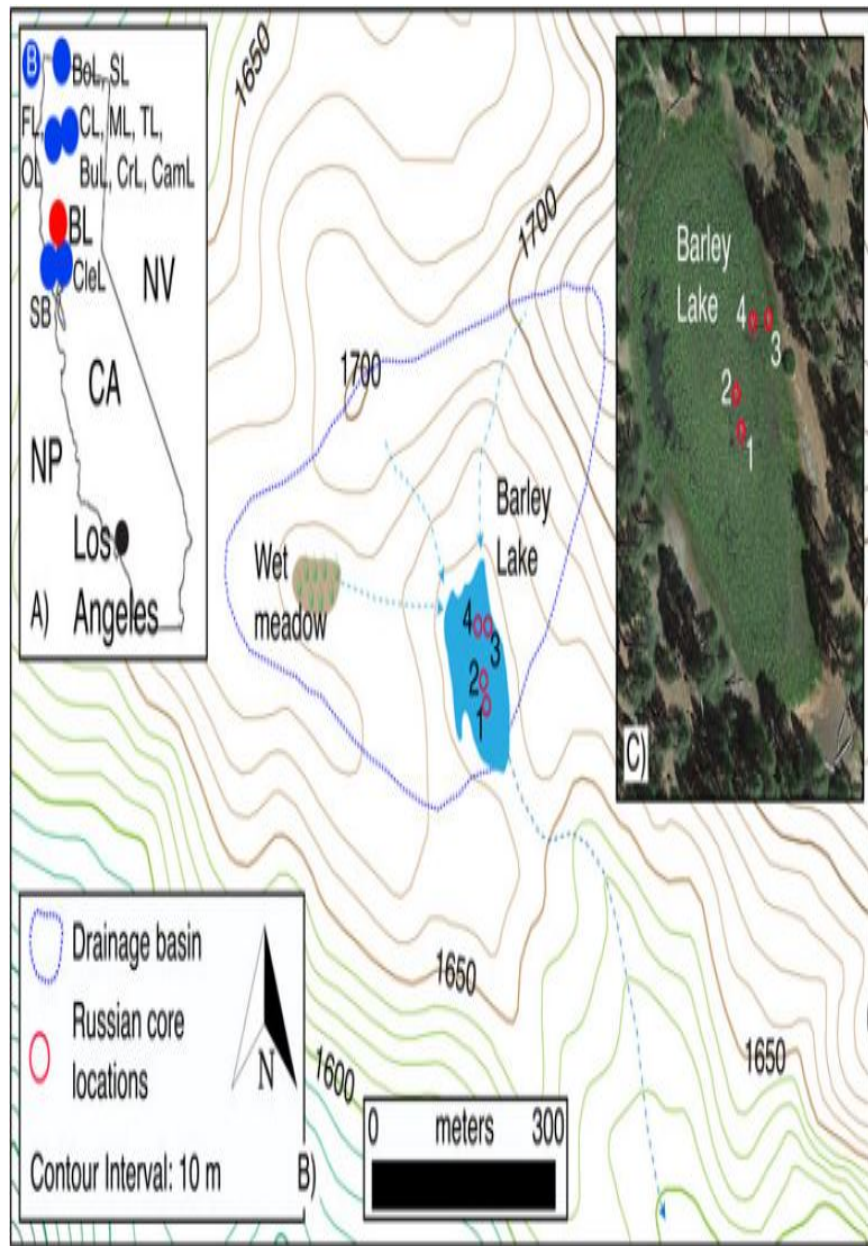


Figure 1: Map of Barley Lake with marked coring locations, BLRC17-1,BLRC17-2,BLRC17-3,BLRC17-4.

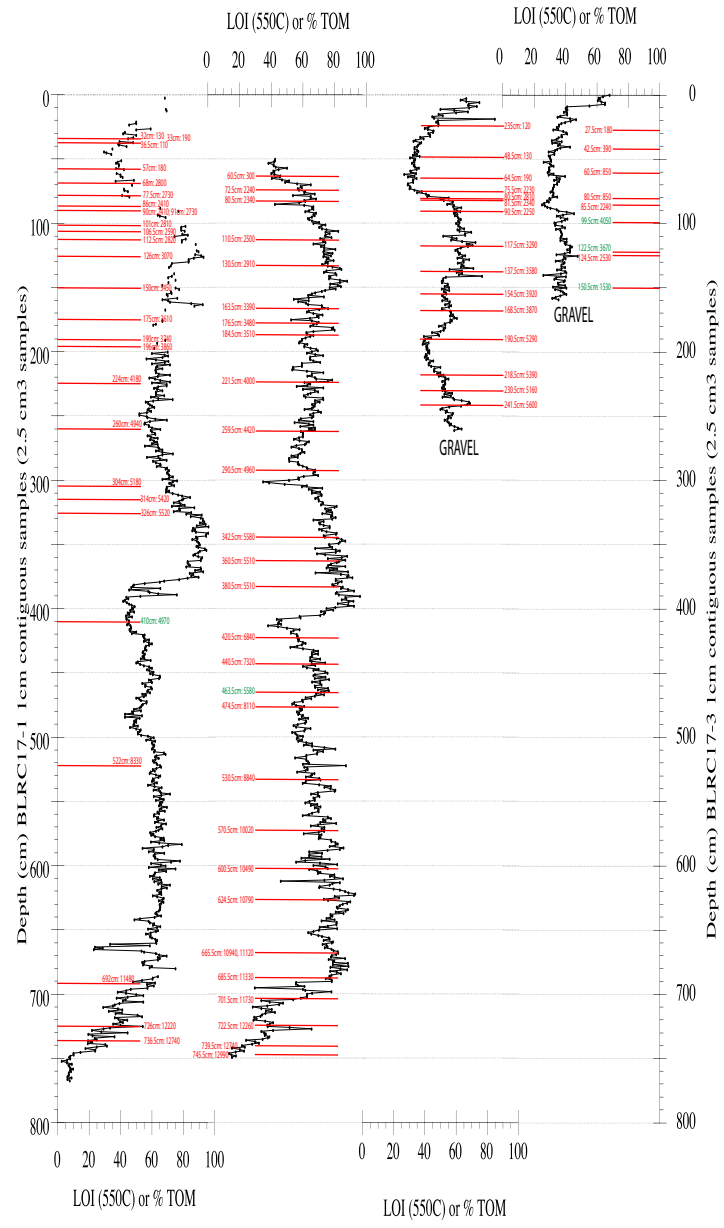


Figure 2: Total Organic Matter % analyzed for each of the four Barley Lake Lacustrine Cores.

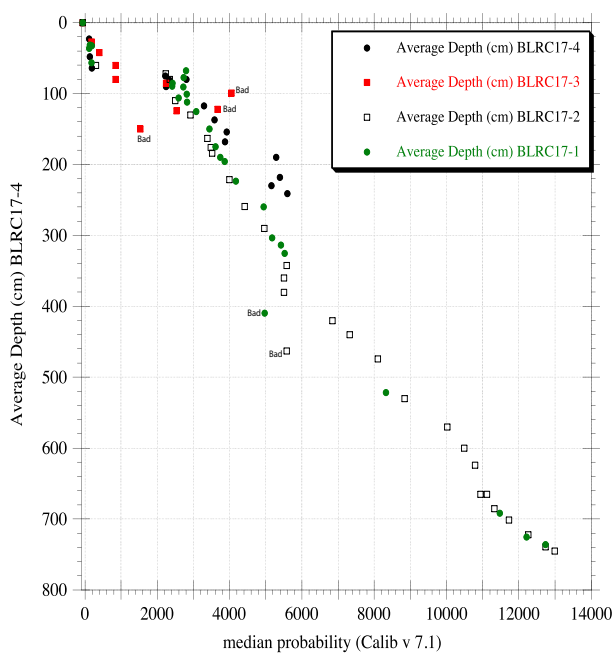


Figure 3: Average Mean Age vs. Depth for carbon-dated organic materials across the four Barley Lake samples.

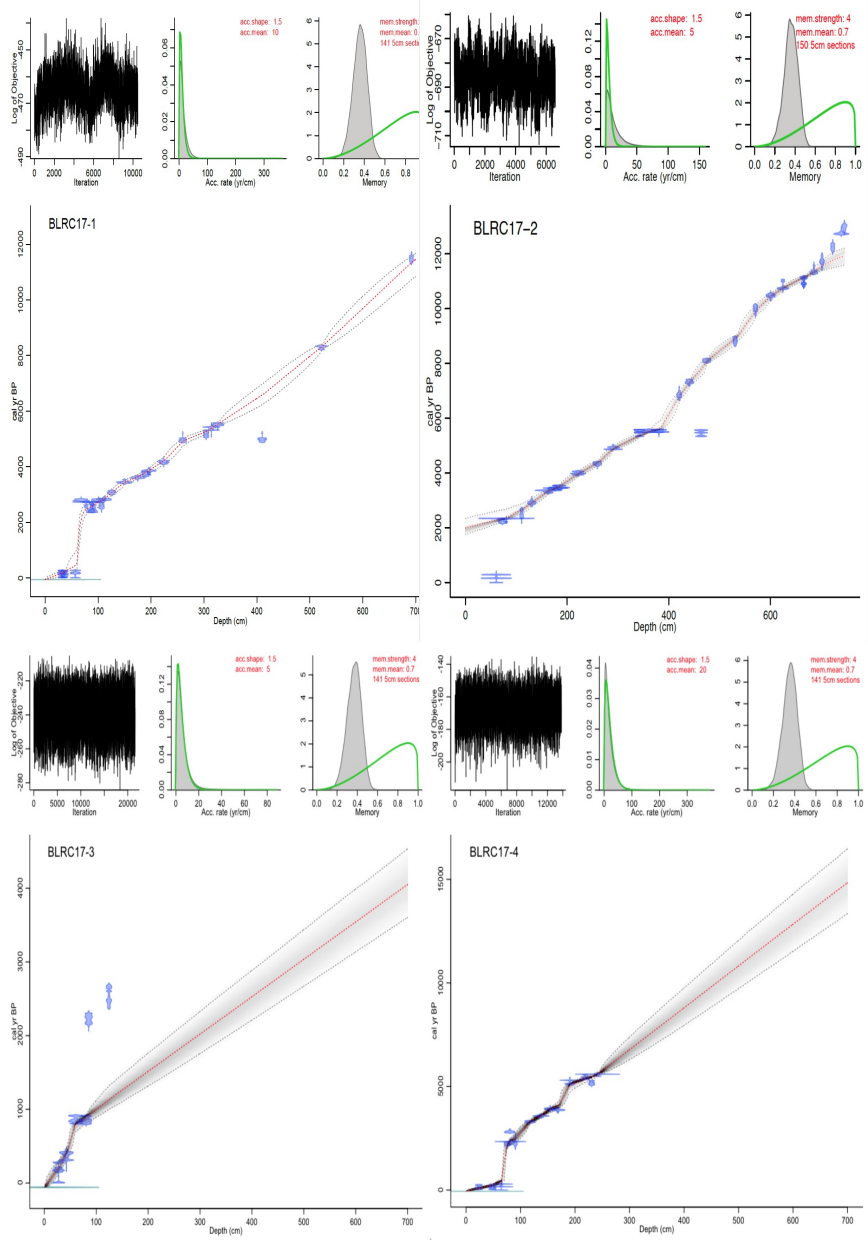


Figure 4: Bacon ghost plots empirically representing age-depth probability densities for each of the four Barley Lake samples. Empirical distributions represented by 6000 posterior samples from the MCMC algorithm.

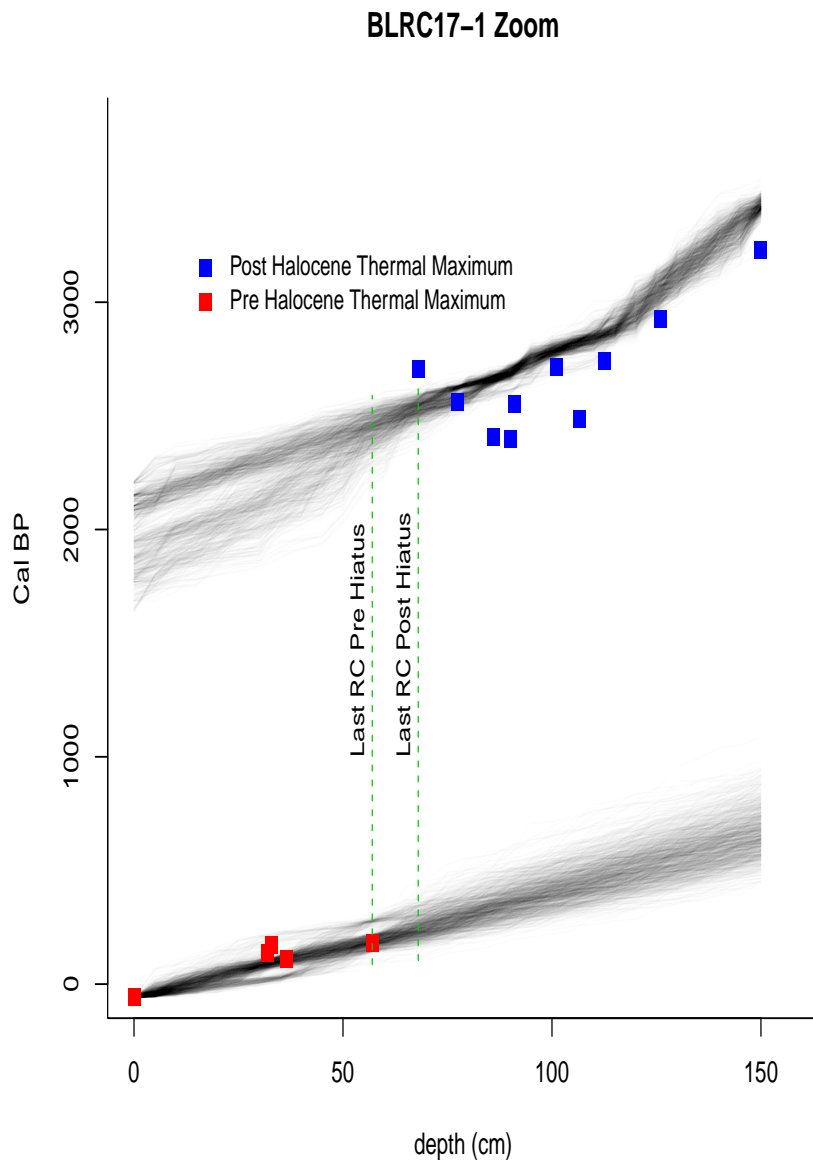


Figure 5: Illustration of process for determining the Bivariate distribution of $g_1(d^*), g_2(d^*)$ using BLRC17-1 and $d^* = 64.5$ cm.

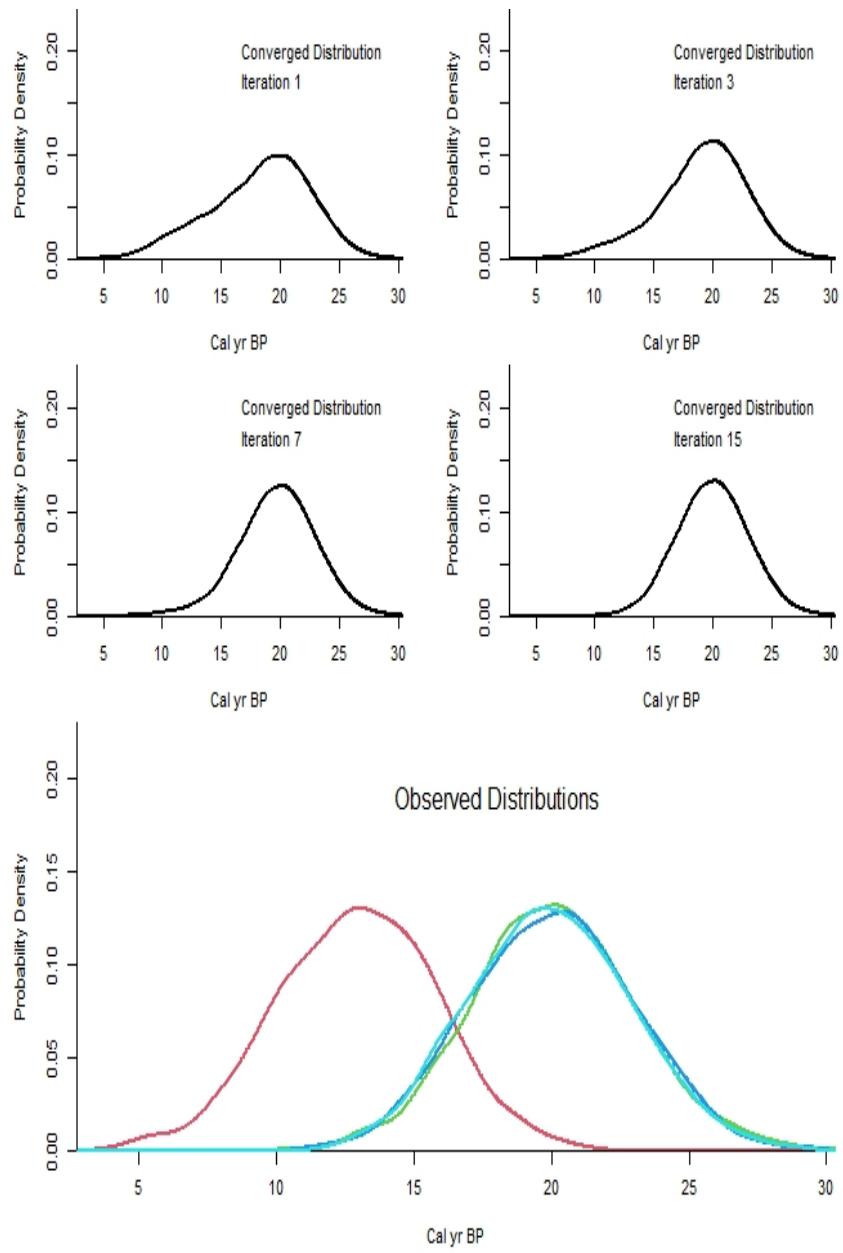


Figure 6: Example result of density congruence methodology for scenario (2).

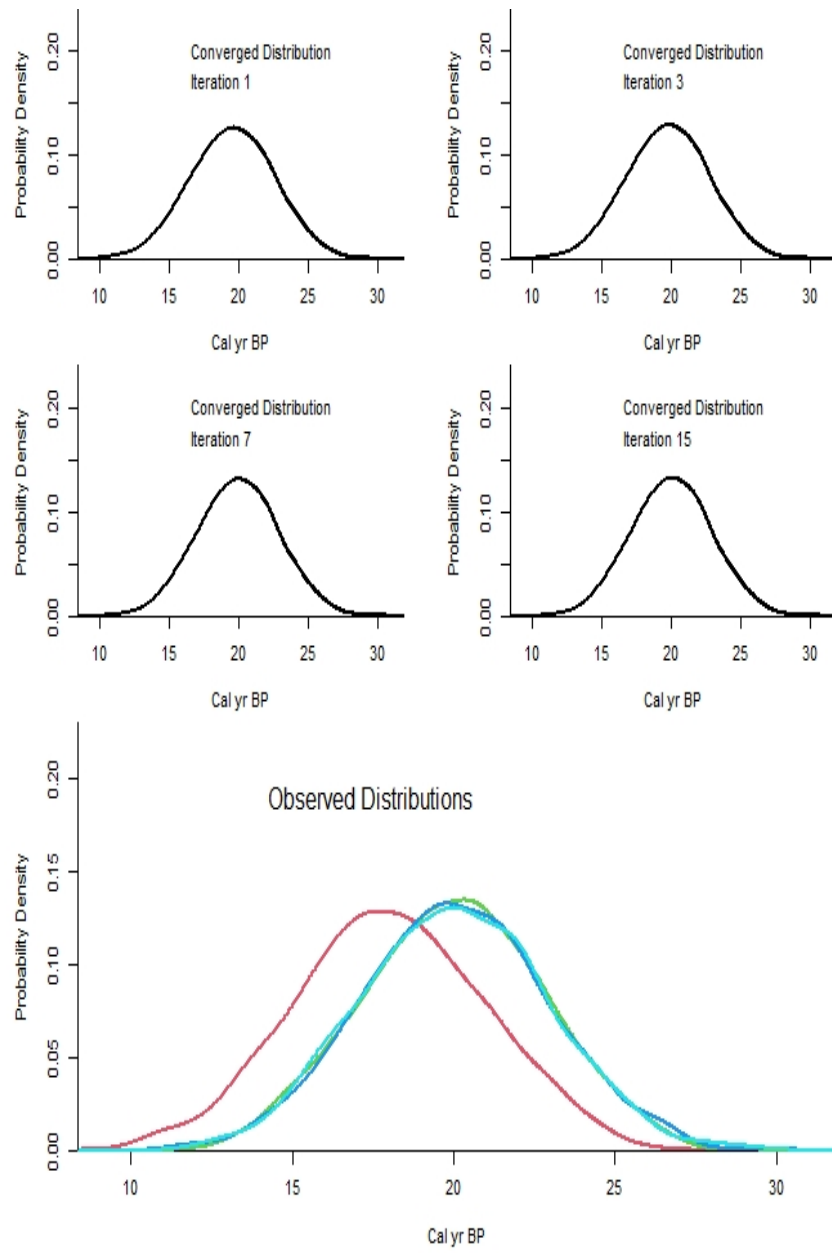


Figure 7: Example result of density congruence methodology for scenario (3).

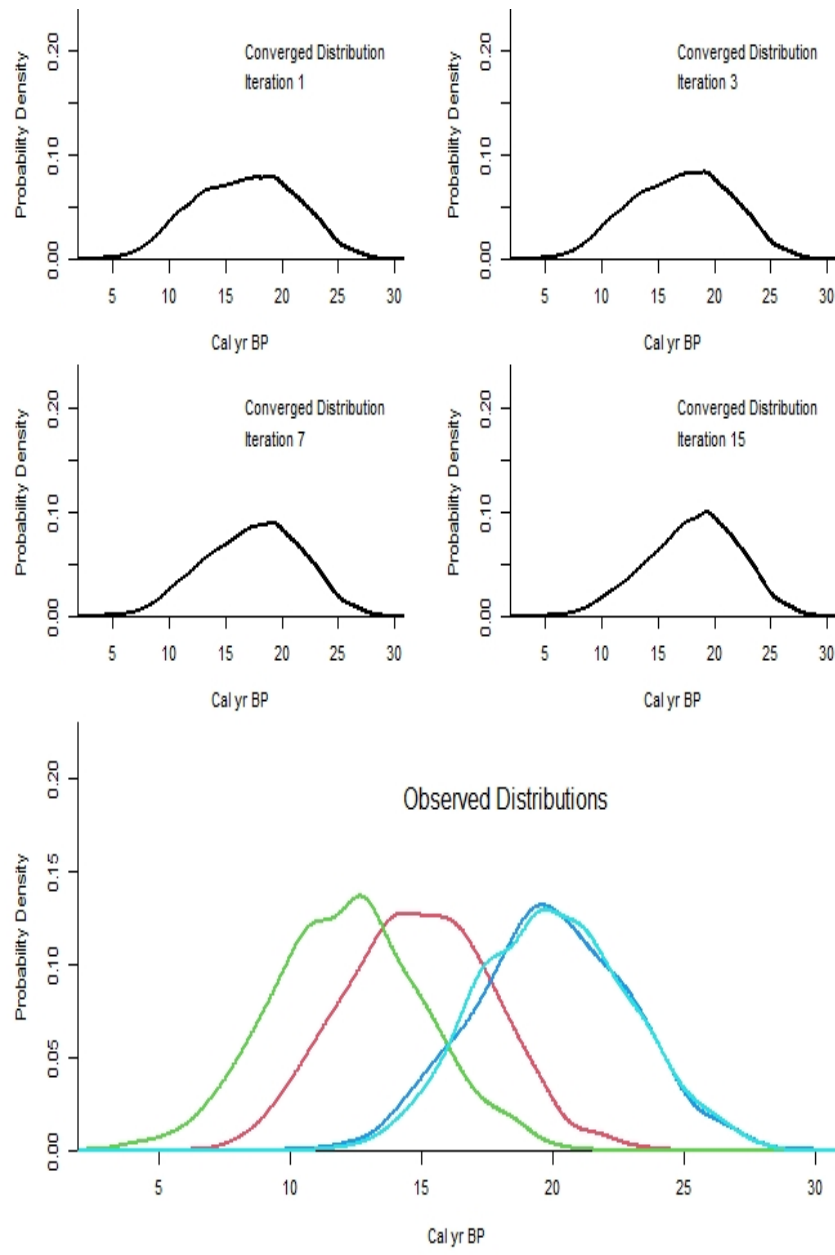


Figure 8: Example result of density congruence methodology for scenario (4).

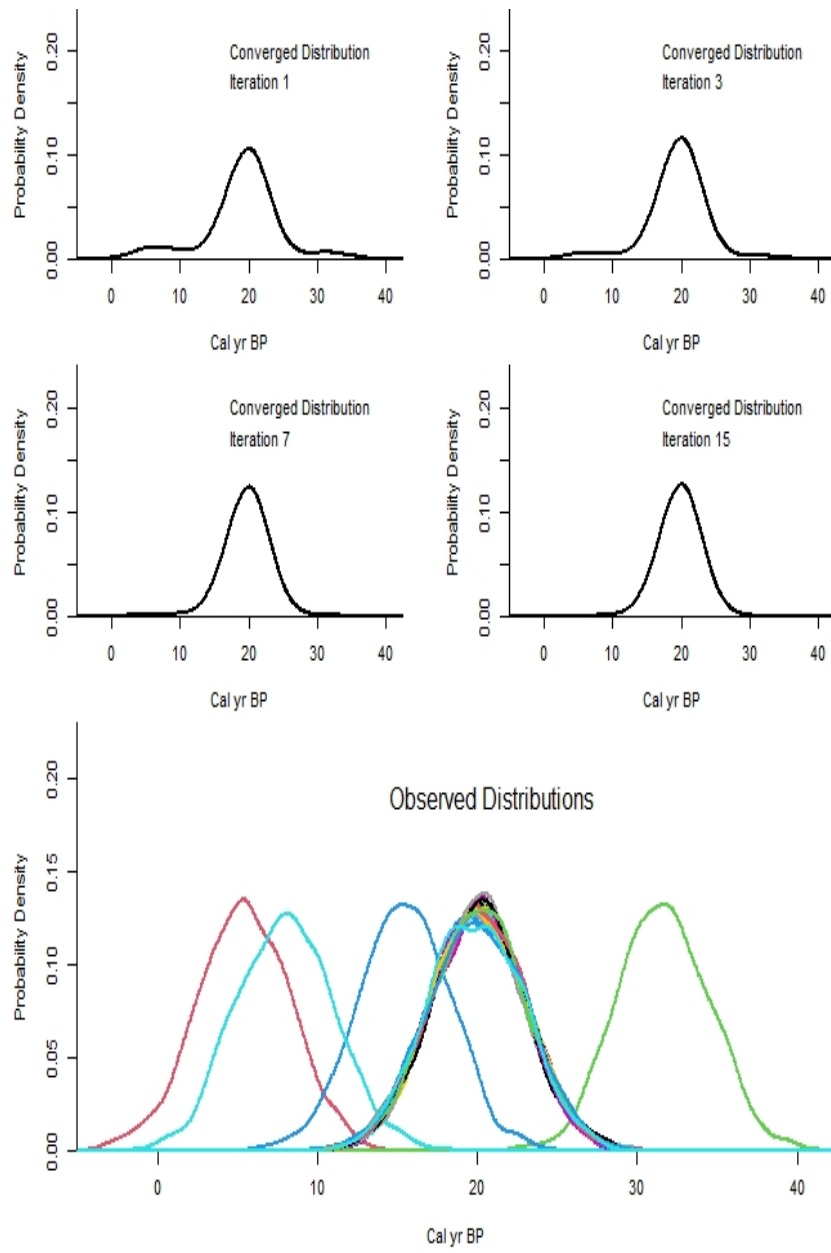


Figure 9: Example result of density congruence methodology for scenario (6).

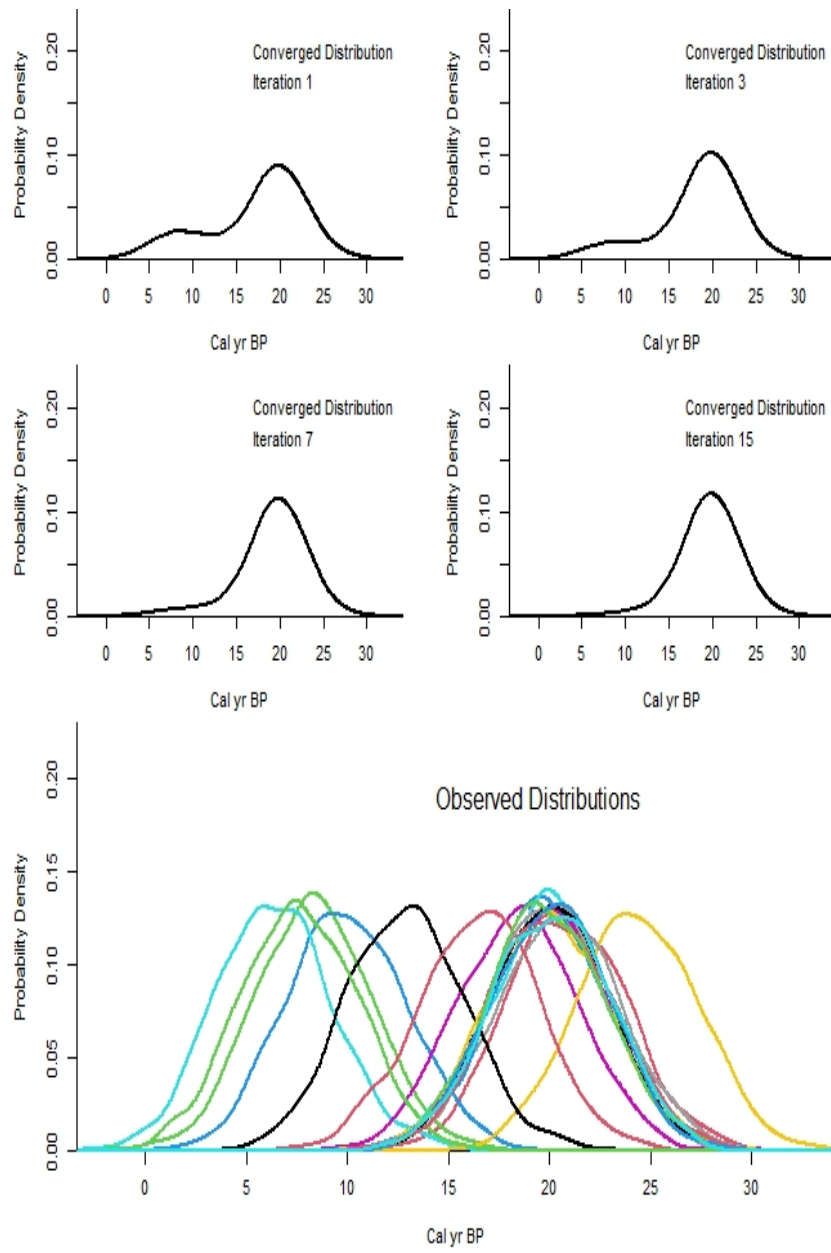


Figure 10: Example result of density congruence methodology for scenario (7).

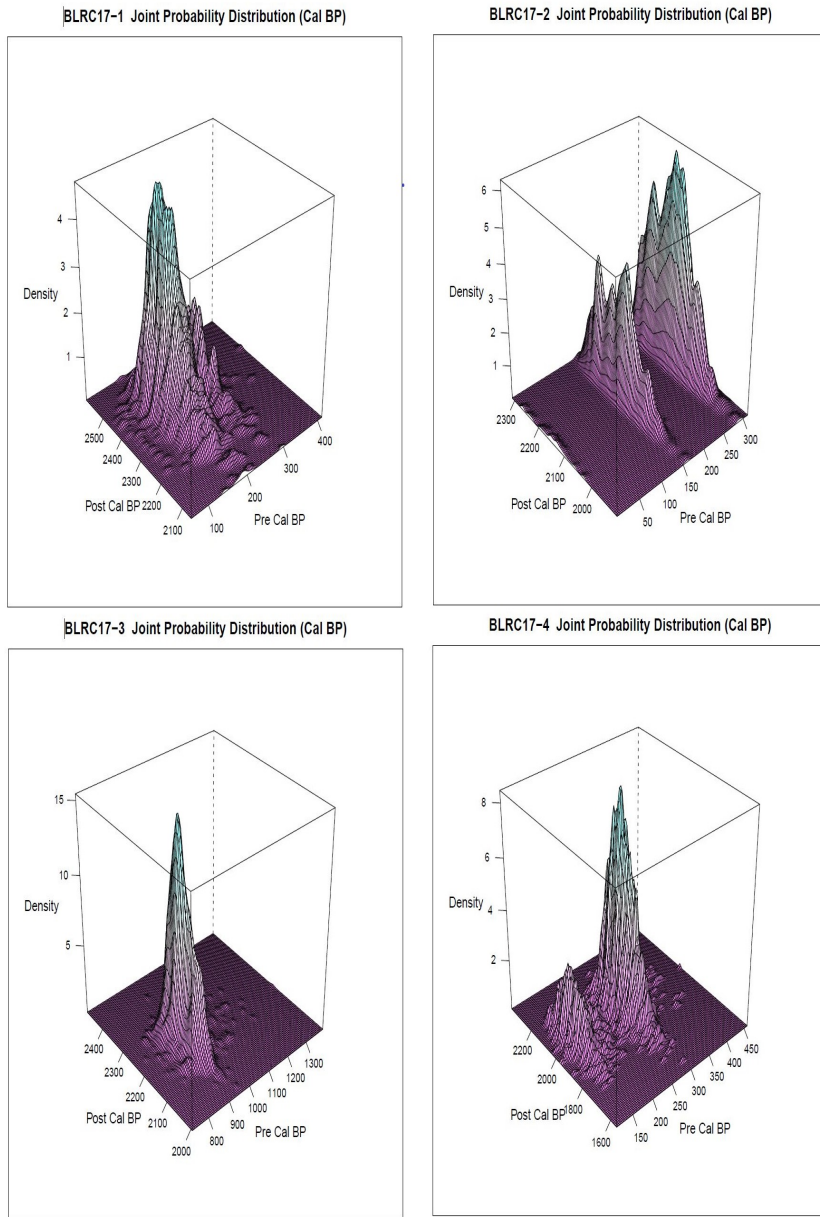


Figure 11: Empirical Bivariate distribution of $g_1(d^*), g_2(d^*)$ for BLRC17-1,BLRC17-2,BLRC17-3,BLRC17-4.

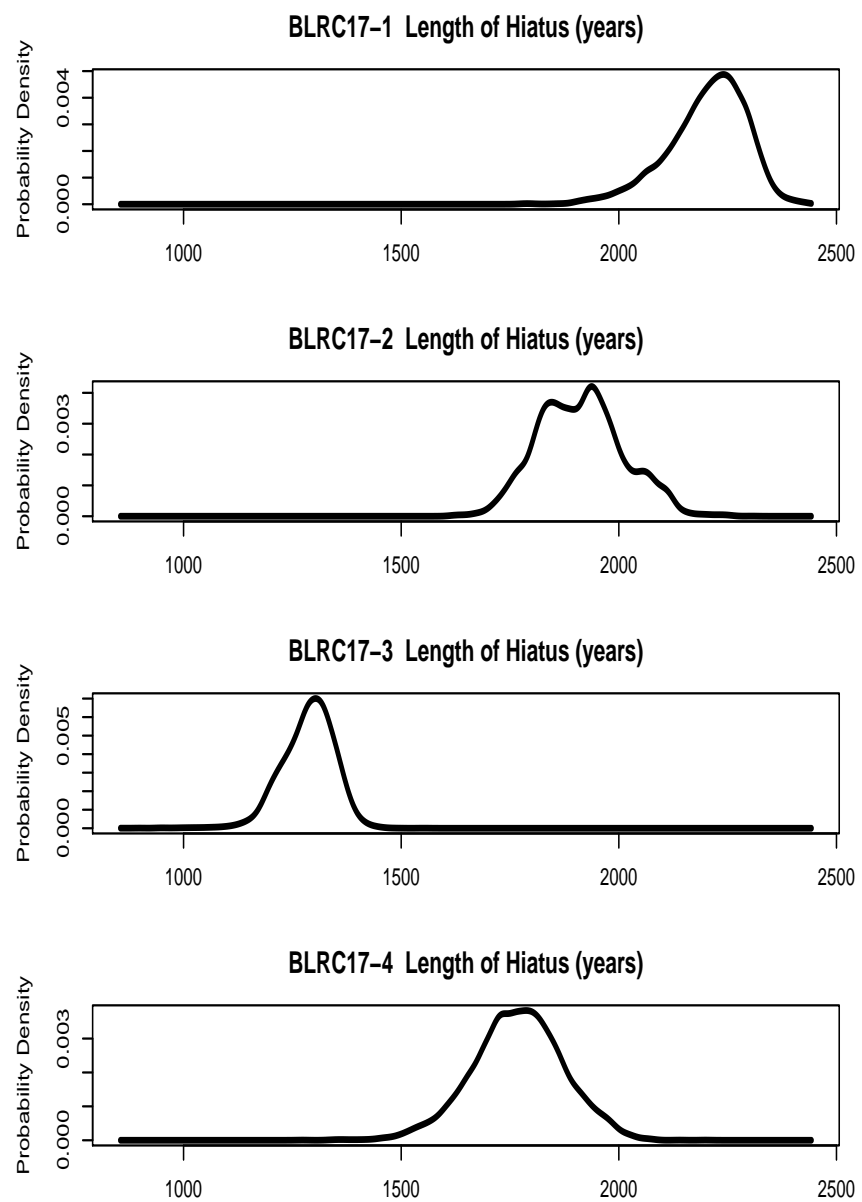


Figure 12: Estimated Probability Density functions for late Holocene hiatus for BLRC17-1, BLRC17-2, BLRC17-3, BLRC17-4.

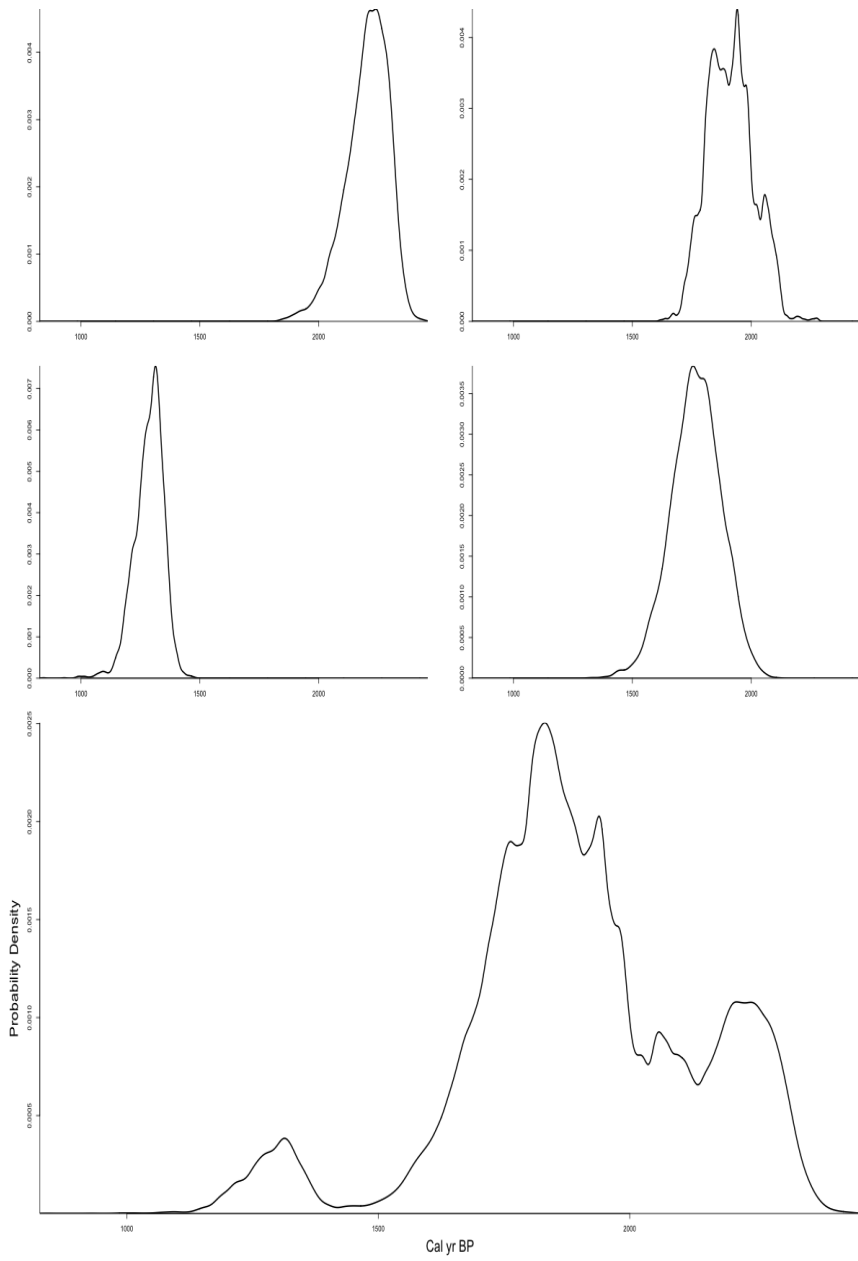


Figure 13: Estimated congruence distribution of the late Holocene hiatus based on BLRC17-1,BLRC17-2,BLRC17-3,BLRC17-4.